JACS
JOURNAL OF THE AMERICAN CHEMICAL SOCIETY
pubs.acs.org/JACS
Article

Flexible Client-Dependent Cages in the Assembly Landscape of the Periplasmic Protease-Chaperone DegP

Robert W. Harkness,*,# Zev A. Ripstein,# Justin M. Di Trani, and Lewis E. Kay*

Cite This: J. Am. Chem. Soc. 2023, 145, 13015−13026
Read Online
ACCESS | Metrics & More | Article Recommendations | Supporting Information

ABSTRACT: The periplasmic protein DegP, which is implicated in virulence factor transport leading to pathogenicity, is a bi-functional protease and chaperone that helps to maintain protein homeostasis in Gram-negative bacteria and is essential to bacterial survival under stress conditions. To perform these functions, DegP captures clients inside cage-like structures, which we have recently shown to form through the reorganization of high-order preformed apo oligomers, consisting of trimeric building blocks, that are structurally distinct from client-bound cages. Our previous studies suggested that these apo oligomers may allow DegP to encapsulate clients of various sizes under protein folding stresses by forming ensembles that can include extremely large cage particles, but how this occurs remains an open question. To explore the relation between cage and substrate sizes, we engineered a series of DegP clients of increasing hydrodynamic radii and analyzed their influence on DegP cage formation. We used dynamic light scattering and cryogenic electron microscopy to characterize the hydrodynamic properties and structures of the DegP cages that are adopted in response to each client. We present a series of density maps and structural models that include those for novel particles of approximately 30 and 60 monomers. Key interactions between DegP trimers and the bound clients that stabilize the cage assemblies and prime the clients for catalysis are revealed. We also provide evidence that DegP can form cages which approach subcellular organelles in terms of size.

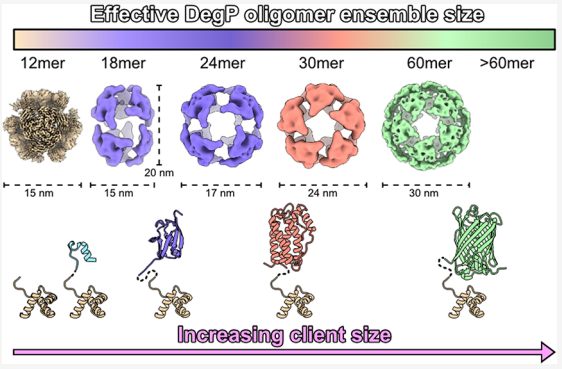

INTRODUCTION

The cellular protein homeostasis network ensures that proteins achieve their native structure and are localized and degraded in a tightly regulated manner.[1,2] Defects in this quality control mechanism lead to the misfolding and aggregation of protein molecules and, ultimately, to cell death.[3] To promote the proper folding and recycling of proteins, cells express an array of protein chaperones and proteases.[4] Some proteins have both functionalities, thus providing client substrates with the chance to refold prior to being recycled if refolding is unproductive. For example, some members of the widely conserved family of High-temperature requirement A (HtrA) proteins[5−7] operate as bi-functional proteases and chaperones that are critical to maintaining cellular fitness and are additionally involved in cell motility, division, and programmed cell death.[8]

DegP is one of the bacterial orthologues of the HtrA protein family that includes members of the antibiotic-resistant ESKAPE pathogens which have been declared a global threat to human health.[9] It operates within the periplasmic space of Gram-negative bacteria, becoming overexpressed in response to a variety of cellular stressors such as heat,[10] oxidative,[11] and osmotic shock,[12] and DegP-null cell lines are growth defective under stressed conditions,[13] underscoring DegP's critical protective function. In conjunction with its role in general periplasmic protein quality control, DegP has been implicated as a major contributor to bacterial pathogenicity due to its participation in shuttling virulence factors to the outer membrane[14−17] where they can be embedded or efficiently secreted to the extracellular space to interfere with the function of neighboring host cells. Clients of DegP include outer membrane proteins (OMPs)[18] and autotransporters[15,19,20] which are collectively involved in nutrient uptake, toxin export, host immune system evasion, and adhesion, among other virulence functions.[15,21,22] The virulence-promoting aspect of DegP function makes it an important target for the development of novel antibiotics as drugs that modulate DegP's interactions with clients could restrict the severity of bacterial infections and promote clearance by the human immune system.[23]

Structurally, mature DegP monomers (lacking the N-terminal periplasmic localization sequence that is cleaved upon entry to the periplasm) contain a serine protease domain

Received: November 7, 2022
Published: June 7, 2023

ACS Publications
© 2023 American Chemical Society

https://doi.org/10.1021/jacs.2c11849
J. Am. Chem. Soc. 2023, 145, 13015−13026

followed by two PDZ domains (Figure 1A top).[6] Three monomers become tightly associated via protease:protease domain interactions to yield a trimeric building block as the basic DegP functional unit with the PDZ1 and PDZ2 domains of each monomer oriented toward the trimer exterior (Figure 1A).[6] Long loops within the protease domains, in addition to flexible linkers connecting the protease-PDZ1 and PDZ1-PDZ2 domains, provide DegP with a remarkable structural plasticity that facilitates the formation of higher-order oligomeric states which have been implicated in DegP function (Figure 1A bottom).[24−26] Classically, the DegP structure−function paradigm was interpreted in terms of structural transitions between an apo resting hexamer state and substrate-engaged cage-like oligomers featuring 12 or 24 monomers that are catalytically active.[27] The resting hexamer structure, solved by X-ray crystallography,[6] was found to form through inter-trimer protease:protease interactions and PDZ1^{i}:PDZ1^{j} domain interactions (in what follows, we will distinguish domains from separate trimers by the subscripts i and j, $i \neq j$). In this state, the PDZ1 and protease domain binding sites are occluded, thus mitigating the unwanted access and subsequent proteolysis of client proteins. An additional "open" hexamer structure was also solved, which was thought to allow for initial substrate engagement.[6] Subsequent structural studies revealed that client binding to the PDZ1 and protease domains causes the reassembly of DegP trimers into cage-like 12mer and 24mer structures that are mediated by PDZ1^{i}:PDZ2^{j} interactions (Figure 1B).[18,24,25,27] These forms of DegP have been shown to proteolyze clients,[27] yet they can also chaperone OMPs.[18] The interplay between these two contrasting DegP functions is not currently well understood.

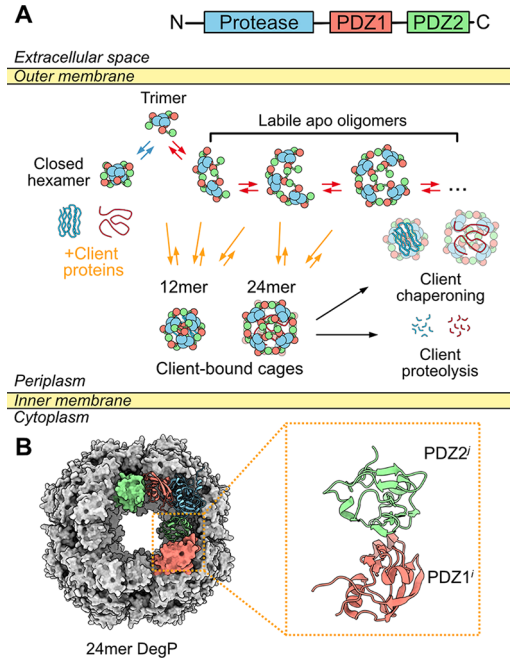

Figure 1. DegP forms client-dependent higher-order oligomers through inter-trimer PDZ domain interactions. (A) Mature DegP monomers contain a serine protease domain (blue) followed by two PDZ domains (PDZ1 in orange and PDZ2 in green, top). Three monomers associate via protease domain interactions to form trimeric building blocks that give rise to higher-order oligomeric architectures through inter-trimer PDZ1^{i}:PDZ2^{j} domain interactions (bottom).[18,25,28] In the absence of substrates, DegP trimers assemble into a broadly populated ensemble of higher-order structures that are structurally distinct from bound cage conformations.[28] Upon substrate engagement, these apo oligomers reorganize into discrete cages, such as the 12mer or 24mer depicted here in cartoon form, which encapsulate the client.[18] (B) Crystal structure of the octahedral 24mer cage (PDB 3MH6,[24] shown in gray surface representation) viewed down the 4-fold axis. Four of the eight trimers comprising the 24mer cage can be seen in the foreground of the image. A single protomer from the top right trimer, colored according to (A), is shown in ribbon representation, highlighting the relative protease/PDZ1/PDZ2 domain orientations in the context of the 24mer cage structure. This protomer is stabilized by an interaction between its PDZ2 domain (green ribbon) and an adjacent PDZ1 domain from a protomer in a second trimer located on the bottom right (shown as an orange surface), referred to as a PDZ1^{i}:PDZ2^{j} interaction (enlarged to the right). A second such interaction is formed, involving the PDZ1 domain from the initial protomer (red ribbon) and an adjacent PDZ2 domain (green surface) from a protomer in a third trimer (top left). This series of PDZ1^{i}:PDZ2^{j} interfaces continues along the front face of the 24mer, returning to the initial interaction site after 4 successive contacts.

Recently, we have shown that in solution and in the absence of substrates, DegP populates a rapidly interconverting stress-dependent distribution of oligomeric states mediated by the weak self-assembly of trimers (Figure 1A bottom).[28] The assembly landscape could be described in terms of two competing oligomerization pathways, one of which leads to the formation of the canonical hexameric state and the other giving rise to a broadly populated ensemble of oligomers that are distinct from canonical, substrate-bound, cage conformers. Our data suggested that the ability to form this highly dynamic oligomeric ensemble composed of partly structured assemblies allows DegP to quickly respond to biological insults by engaging client proteins and reassembling into discrete cage conformers for substrate processing. Interestingly, our prior work implied that in the apo state, oligomeric ensembles of DegP can have effective molecular weights exceeding ∼3 MDa, corresponding to >60mer particles that are much larger than any known cage structures. We thus asked whether DegP actually forms cages of this size. Such large cage conformers may be of biological importance, for example, in the chaperoning of high molecular weight clients including autotransporter virulence factors, which are often ∼100−200 kDa in size.[22,29,30] Furthermore, DegP likely encounters substrates of many sizes in the periplasm, and the ability to form a continuum of cage-like conformations, both apo- and client-bound, would enable a functional flexibility for responding to protein misfolding stresses. Here, we have explored the types of cages that are adopted by DegP in response to substrates of different sizes. This was achieved through a recombinant client protein engineering approach in which we attached a known DegP binding motif to the C-terminus of a series of folded proteins of increasing hydrodynamic radii. We then analyzed the types of DegP cages formed in the presence of these chimeric clients using a combination of dynamic light scattering (DLS) and cryogenic electron microscopy (cryo-EM). We find a correlation between the size distribution of cage particles adopted by DegP and the size of the engaged substrate protein and herein present a series of client-engaged structures including 30mer and 60mer cages. These reveal novel interactions between DegP trimers and bound clients that stabilize DegP cages and prime substrates for cleavage by the protease domains. We additionally provide evidence that, in the presence of large substrate

https://doi.org/10.1021/jacs.2c11849
J. Am. Chem. Soc. 2023, 145, 13015−13026

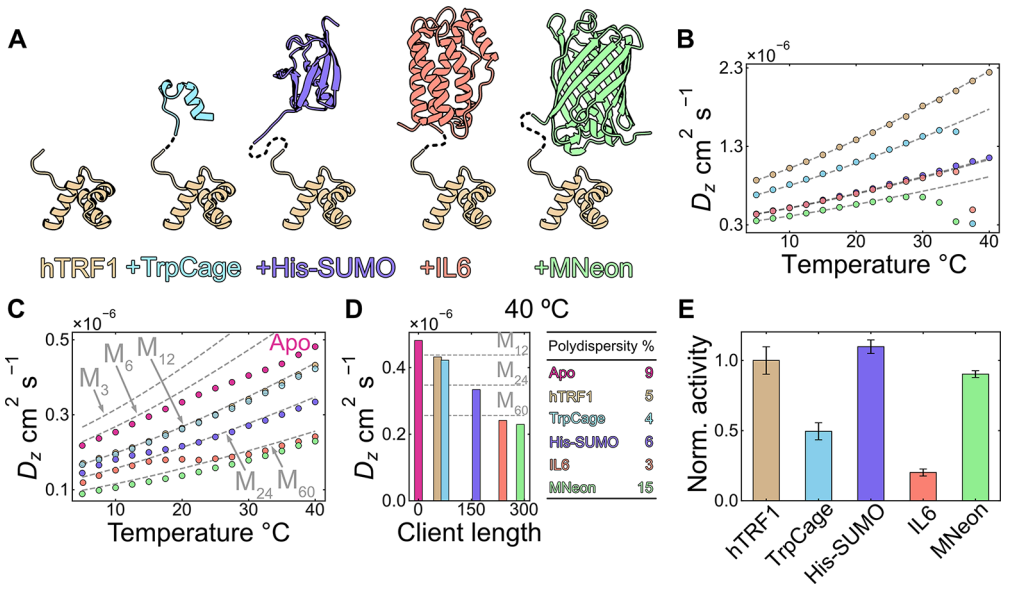

Figure 2. Characterization of engineered DegP clients and their influence on DegP oligomerization by DLS. (A) DegP substrates have been engineered with an hTRF1 binding tag (tan, PDB 1ITY[34]) C-terminal to folded proteins of increasing hydrodynamic radii (TrpCage, PDB 1L2Y,[35] His-SUMO, PDB 1EUV,[36] IL6, PDB 2IL6,[37] and MNeon, PDB 5LTR,[38] in blue, purple, orange, and green, respectively). (B) D_z values (colored points) for the substrates in (A) measured as a function of temperature by DLS. Note that certain substrates (TrpCage, IL6, MNeon) undergo irreversible unfolding/aggregation at high temperature (~30−40 °C), leading to sharp decreases in measured D_z values. Hydrodynamic radii (r_h) for each substrate (1.5, 1.9, 3.0, 3.0, and 3.7 nm, respectively) have been calculated from their D_z values at 5 °C (in the absence of unfolding/aggregation) and used to generate temperature-dependent D_0 profiles to guide the eye (gray dashed lines) using the Stokes−Einstein relationship. (C) D_z values for S210A DegP (100 μM protomer concentration) in the presence of 200 μM of each of the substrates in (A). D_z values for apo DegP (no added substrate) are shown in red for comparison. D_0 values (gray dashed lines) calculated for 3mer, 6mer, 12mer, 24mer, and 60mer DegP particles are indicated. In the case of the 3mer, 6mer, and 12mer, r_hs of 4.9, 5.7, and 7.8 nm, respectively, were obtained from D_z values measured at low temperature[28] and then used to generate the $D_0(T)$ profiles shown via the Stokes−Einstein equation. The profiles for the 24mer and 60mer oligomers were calculated from a scaling law for spherical particles that relates $D_0(T)$ values to the number of DegP 3mers according to $D_{3N,0}(T) = D_{3,0}(T) \times N^{-1/3}$, where $D_{3,0}(T)$ is the 3mer diffusion constant, N is the number of 3mers (=8 for the 24mer and 20 for the 60mer), and the −1/3 exponent accounts for the particle shape.[28,39] (D, left) D_z values from (C) at 40 °C as a function of the client polypeptide chain length. D_0 values for 12mer, 24mer, and 60mer particles are shown as horizontal gray dashed lines. (D, right) Polydispersity percentages associated with the D_z values in (D, left), calculated as $100 \times \sigma^2/\mu^2$, where μ and σ are derived from cumulants analysis of the DLS data.[40] Here, μ is the average autocorrelation function relaxation rate ($\propto D_z^2$) and σ is the standard deviation of the relaxation rate distribution. Polydispersity percentages are thus measures of the variance of the diffusion constant distribution for the solution ensemble relative to the mean squared value. (E) Normalized cleavage rates for the substrates in (A) in the presence of proteolytically active DegP. The cleavage activities for the engineered substrates have been normalized to the value for hTRF1 (see Supporting Information). Bar heights are given as the mean ± SD from triplicate activity measurements.

proteins, DegP can form oligomeric structures that approach subcellular organelles in terms of size.

RESULTS

Characterizing Engineered DegP Substrates and Their Influence on DegP Cage Distributions by DLS. DegP engages partially or fully unfolded client proteins via their C-termini,[31] leaving their N-terminal portions unbound and, presumably, projected toward the interior of the cages. The unbound portions of clients are typically not observed in the structures of DegP cages due to their flexibility. We hypothesized that by increasing the size of the N-terminal, free portion of the engaged substrate, DegP would be forced to adopt increasingly larger cages in order to accommodate clients within the cage interiors. We thus selected a series of folded proteins (TrpCage, His-SUMO, IL6, and MNeon) of increasing hydrodynamic radii (r_h) to explore the influence of substrate size on the types of cages adopted by DegP (Figure 2A). To ensure binding to DegP and provide each substrate with a standard interaction motif, each of these proteins was engineered to contain a known C-terminal DegP affinity tag. Here, we selected the DNA binding domain of the human telomere repeat binding factor (hTRF1, 54 residues).[32] In what follows, we refer to these engineered chimeric constructs, for example, as TrpCage-hTRF1 to denote their fusion to the C-terminal hTRF1 tag (see Table S1 for their amino acid sequences). Our choice of hTRF1 as the scaffold for investigating the types of DegP particles formed in response to uptake of clients of different sizes was motivated by our previous study showing that hTRF1 interacts with DegP with high affinity (i.e., complete binding saturation at ~1:1 protomer:substrate molar ratio).[28] Prior studies of DegP-client interactions focused on denatured proteins,[26] disordered protein fragments,[25] and short peptides[33] as model interaction systems. In contrast, structural studies of hTRF1 with DegP provide an opportunity to fill a noticeable gap in the literature by obtaining unique insights into DegP:natively folded substrate interactions, addressing, for example, whether hTRF1 is fully unfolded in the bound state or whether residual structure or non-native conformations are present.

To explore the influence of the substrates on DegP oligomerization, we measured DLS datasets from which we extracted z-average diffusion constants (D_z). When a particle distribution consists of species of somewhat similar sizes (within a factor of ~5[41]), as would be the case for DegP:client samples consisting of cage architectures and/or partly

https://doi.org/10.1021/jacs.2c11849
J. Am. Chem. Soc. 2023, 145, 13015−13026

assembled intermediate species, the measured DLS data are well described by a single D_z value which corresponds to an average of the diffusion constants for each species in solution weighted by their relative light scattering intensities.[41−43] Thus, comparisons of D_z values as a function of added client or solution conditions, such as temperature, provide insight into the nature of the DegP ensembles at hand. For example, we have previously shown D_z values to be sensitive reporters of the higher-order oligomers that are formed by DegP in the absence and presence of client proteins such as hTRF1.[28] In this study, we have extended our earlier approach, which utilizes a plate reader format DLS instrument, to screen in a high-throughput manner for changes to DegP's oligomeric distribution in response to client binding. This strategy enabled us to investigate multiple client concentrations and solution temperatures in a single experiment and thereby explore a wide range of conditions under which DegP is thought to act as a stress-protective protease and chaperone.[5,11,44] Initially, D_z values for each of the five substrates in Figure 2A were obtained as a function of temperature (5−40 °C) to evaluate their hydrodynamic size and thermal stability (Figure 2B). As expected, we found a clear correlation between the extracted D_z values and the size of the substrate, with smaller substrates diffusing faster than larger ones, according to $D_{z,\text{hTRF1}} > D_{z,\text{TrpCage-hTRF1}} > D_{z,\text{His-SUMO-hTRF1}} \approx D_{z,\text{IL6-hTRF1}} > D_{z,\text{MNeon-hTRF1}}$ over the temperature range of ∼5−30 °C. Certain substrates (TrpCage-hTRF1, IL6-hTRF1, and MNeon-hTRF1) were found to undergo irreversible unfolding and/or aggregation beyond these temperatures, as evidenced by their DLS autocorrelation functions (Figure S1A−E, left). The dramatic shifts to longer autocorrelation function decay times and the appearance of multiphasic behavior and noisy baselines at these temperatures are consistent with the formation of multiple large and heterogeneous scattering species corresponding to high molecular weight protein aggregates.[45] In these cases, the multimodality of the particle distribution cannot be accounted for with a single D_z value, leading to poor fits of the autocorrelation functions with this analysis (Figure S1B,D,E, left). The aggregation of the sample, shifting the autocorrelation decay to much longer timescales, gives rise to the steeply decreasing and anomalously small extracted D_z values that are shown in Figure 2B over the range of ∼30−40 °C.

We then obtained D_z values for proteolytically inactive S210A DegP (to prevent auto and substrate catalysis) in the presence of each substrate as a function of temperature (5−40 °C, Figures 2C and S2; colored circles for client-bound data match the client colors in Figure 2A,B). We selected a 100 μM S210A DegP protomer concentration since this is within the experimentally determined biological range for DegP in the *E. coli* periplasmic space[28] and used three concentrations of each substrate (50, 100, and 200 μM) to assess cage formation at several molar ratios of DegP:substrate (Figures 2C and S2; note that in Figure 2C, only the 1:2 monomer:monomer data are shown for clarity). As the substrates are small relative to DegP trimers and cages (∼7 to 33 kDa vs ∼140 kDa for a DegP trimer as the smallest DegP oligomer; note that this mass difference increases dramatically upon the formation of larger, client-engaged DegP species) and are not in dramatic molar excess even at the highest employed concentration, the contribution of any unbound client to the D_z values is negligible. Therefore, the extracted D_z values are direct reporters of the formation of client-engaged DegP particles.[28]

A sample of apo DegP at 100 μM protomer concentration was also included as a reference, highlighting DegP's oligomeric distribution in the absence of a substrate (Figure 2C, red circles). The D_z values for DegP in the absence and presence of the five substrates followed $D_{z,\text{DegP}} > D_{z,\text{DegP+hTRF1}} \approx D_{z,\text{DegP+TrpCage-hTRF1}} > D_{z,\text{DegP+His-SUMO-hTRF1}} > D_{z,\text{DegP+IL6-hTRF1}} > D_{z,\text{DegP+MNeon-hTRF1}}$ at all temperatures, suggesting the formation of different oligomer distributions depending on the size of the N-terminal portion of the bound client (Figure 2C,D, left). Interestingly, the measured autocorrelation decays for the DegP particle distributions generated with either small (e.g., hTRF1) or large (e.g., MNeon-hTRF1) clients were narrow and monophasic (Figure S1A−E, right). As mentioned above, this suggests that in each DegP:client sample, the particle distribution consists of oligomers that are similar in size, as otherwise distinct transitions within the autocorrelation functions that correspond to the presence of separate particle distributions with very different average sizes would be observed. To assess the variance of the molecular sizes in the DegP:client samples, we additionally examined the polydispersity values afforded by our DLS analysis (Figure 2D, right). For DegP:hTRF1, DegP:TrpCage-hTRF1, DegP:HisSUMO-hTRF1, and DegP:IL6-hTRF1, these were relatively small (3−6% at 40 °C compared to 9% for apo DegP which is known to populate an array of cage-like, rapidly interconverting species mediated by weak 3mer:3mer interactions[28]) and again consistent with a narrow particle distribution. In contrast to the other client complexes, the polydispersity values for DegP:MNeon-hTRF1 were elevated (15%, Figure 2D, right), pointing to a particle distribution even wider than found for apo DegP, although still monomodal and well described by a single D_z value (Figure S1E, right). Notably, we did not observe changes to the autocorrelation functions for DegP in the presence of the clients over the DLS temperature range that would indicate the formation of nonspecific protein aggregates (Figure S1A−E, right), as was found for apo TrpCage-hTRF1, IL6-hTRF1, and MNeon-hTRF1 (Figure S1B,D,E, left); however, the concentrations of free protein required for accurate measurements of D_z values (Figures 2B, S1A−E, left) are much higher than for the complexes in Figure 2C.

To rule out the possibility that the chimeric substrates could bind to DegP via regions other than the hTRF1 tag, we prepared additional constructs containing only the N-terminal portion of the chimeras (i.e., TrpCage, His-SUMO, IL6, and MNeon) and repeated the DegP binding experiment by DLS (Figure S3). In all cases, the D_z values for S210A DegP in the presence of these constructs did not show any decreases in magnitude and reproduced the profile obtained for the apo S210A DegP reference sample, indicating that cage formation is not induced by these clients without the C-terminal hTRF1 tag. Thus, changes in particle sizes reflect differences in substrate radii and not changes in the mechanism of binding to DegP.

As reference points for estimating the ensemble average size of the DegP particle distributions that are consistent with the D_z values measured in the presence of the clients over the experimental temperature range, we calculated temperature-dependent diffusion constants for a series of DegP oligomers (3mer, 6mer, 12mer, 24mer, and 60mer, gray dashed lines in Figure 2C,D) based on experimentally determined r_h values for 3mer, 6mer, and 12mer particles, or for the 24mer and 60mer species, from a scaling law for spherical particles relating the

https://doi.org/10.1021/jacs.2c11849
J. Am. Chem. Soc. 2023, 145, 13015−13026

diffusion constant to the number of DegP trimers in the higher-order structures.[28,39] Consistent with our previous study on DegP oligomerization in the absence of a substrate,[28] the D_z values for apo DegP under these conditions initially track with those expected for a hexamer at low temperature (~5−15 °C) and then subsequently decrease as the temperature is elevated, reflecting the higher-order apo oligomers that become populated at higher temperatures (~25−40 °C). The $D_{z,\text{DegP+hTRF1}}$ data were consistent with the values expected for a 12mer cage, in agreement with our previous report.[28] D_z values for DegP in the presence of TrpCage-hTRF1 were slightly below the values for hTRF1, possibly the result of the formation of a small amount of larger species that could include 18mer cages in addition to 12mers.[28] For DegP in the presence of the larger substrates (His-SUMO-hTRF1, IL6-hTRF1, and MNeon-hTRF1), we observed fluctuations in the D_z values that were suggestive of substantial redistributions of the DegP oligomer ensembles in response to increasing temperature (Figures 2C and S2). At low temperature (~5−15 °C), D_z values for DegP bound to His-SUMO-hTRF1 are situated between those expected for 12mer and 24mers, consistent with a distribution of particles within approximately this size range. At higher temperatures (~>20 °C), the $D_{z,\text{DegP+His-SUMO-hTRF1}}$ values transition toward and eventually pass slightly below the 24mer values, pointing to the formation of a particle distribution with an average size somewhat larger than 24mers. A similar trend was observed for DegP bound to IL6-hTRF1, except that these D_z values are consistent with a distribution of roughly 24mer-sized species at lower temperature (~5−15 °C), shifting toward and slightly below the values expected for a 60mer at high temperature (~25−40 °C), and indicating the formation of an oligomeric ensemble containing small amounts of even larger species. Finally, the $D_{z,\text{DegP+MNeon-hTRF1}}$ data initially are close to those expected for a 60mer at lower temperatures and deflect below the 60mer line, again pointing to the formation of a small proportion of higher-order particles at high temperatures. The temperature deflections for DegP in the presence of larger substrates may reflect, in part, the unfolding of the hTRF1 subunit of unbound chimeric clients. An increase in the unfolded fraction of the hTRF1 tag would increase the effective binding affinity, as DegP can bind denatured clients preferentially,[31] leading to increased saturation of DegP with temperature. Additional copies of clients populating the DegP binding sites might lead to a redistribution of the ensemble toward larger oligomers due to steric contacts between the bound substrates, ultimately giving rise to the observed deflections in the measured D_z values. Alternatively, formation of larger particles for the His-SUMO-hTRF1, IL6-hTRF1, and MNeon-hTRF1 complexes may simply reflect a temperature-dependent redistribution of the client-engaged oligomeric ensemble in a manner analogous to what occurs with apo DegP.[28] Insight into the dynamics of oligomer formation is, in principle, also available from the analysis of DLS data; however, we were unable to capture the assembly phase of the reactions due to the dead time associated with mixing and centrifuging the samples, and loading the instrument, coupled with the relatively rapid oligomer assembly kinetics (complete within approximately 2 min), as observed in earlier studies of DegP using a fluorescence-based approach.[25]

It should be noted that, although we often refer to each complex in terms of the mean number of monomers it contains in what follows, the complexes should be thought of as ensembles and not as discrete structures. It is important to emphasize that a single distribution is likely an oversimplification, in particular for the larger complexes considered, as has been discussed above. In general, the DLS data cannot distinguish between a single, somewhat broad distribution of structures or multiple, discrete narrower distributions that are overlapped.

Having established that our suite of engineered DegP clients leads to different cage distributions, we next sought to assess how these substrates would be cleaved by protease-active DegP. To obtain a crude estimate of DegP activity toward the clients, we incubated active DegP with each of the substrates at room temperature overnight and analyzed the reaction products using SDS-PAGE (Figure S4). In all cases, we observed hTRF1 cleavage products exclusively, implying that active DegP digests only the hTRF1 tag. This is most evident for the larger substrates (His-SUMO-hTRF1, IL6-hTRF1, MNeon-hTRF1), where low molecular weight bands corresponding to the hTRF1 tag cleavage products are observed in addition to higher molecular weight bands for the free, intact N-terminal portions of these chimeras. To confirm that these cleavage products are the result of C-terminal hTRF1 tag digestion, we subjected the reaction products to LC−MS analysis. A similar product profile for each of the chimeric substrates was observed, with the accompanying peptide masses matching those expected for cleavage of the hTRF1 tag (Table S2). We also measured activity profiles for each of the substrates using changes in the intrinsic fluorescence of hTRF1 as a reporter. These data revealed similar cleavage rates for hTRF1, His-SUMO-hTRF1, and MNeon-hTRF1, while TrpCage-hTRF1 and IL6-hTRF1 were digested at somewhat slower rates (~50 and 20% of the hTRF1 rate, Figure 2E). Differences in activity for the TrpCage-hTRF1 and IL6-hTRF1 constructs support the notion that their N-terminal portions influence DegP protease activity against the bound hTRF1 tag, which could have implications for DegP function in the periplasm (see Discussion section).

Cryo-EM Structural Studies of DegP Cages in the Presence of Engineered Substrates. The correlation between the sizes of the engaged clients and the sizes of the DegP:client particles, as evidenced by the DLS-derived D_z values (Figure 2C,D), prompted us to use single-particle cryo-EM to investigate the structures of the substrate-bound assemblies in more detail. To this end, we prepared samples of the series of five DegP:client complexes (at 100 μM DegP monomer:200 μM client concentrations to ensure saturation of the cages with the substrate) and subjected each to cryo-EM analysis (see Supporting Information, Figures S5−S7). Inspection of the micrographs and 2D class averages for the different complexes examined suggested increasingly large oligomeric ensembles as a function of increasing client size (Figures 3A, S5), in agreement with our macroscopic analyses of the DegP particle distributions by DLS.

In the case of the smallest complex corresponding to the bound hTRF1 substrate, *Ab-initio* reconstruction with three classes led to one map with a clear tetrahedral shape, consistent with the 12mer cage (15 nm diameter) observed previously[28] (Figures 3B, S5A, S6A I and II, ~57% of the selected particles). The particle images from the other two classes were not subject to further analysis as the maps produced in the reconstruction did not depict a well-defined DegP assembly (Figure S6A II). Refinement of the 12mer class with C_1 (equivalent to no symmetry group applied) or tetrahedral

https://doi.org/10.1021/jacs.2c11849
J. Am. Chem. Soc. 2023, 145, 13015−13026

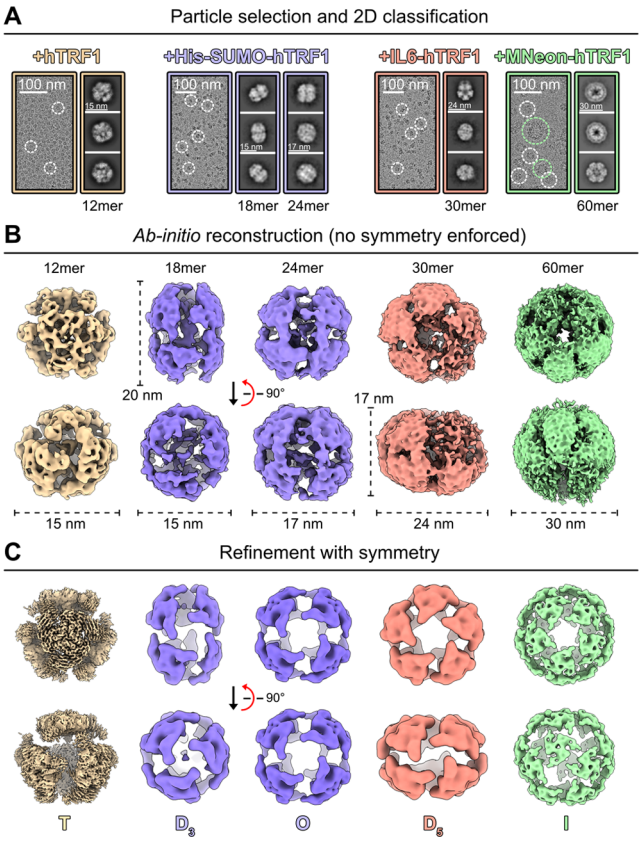

Figure 3. Cryo-EM analysis of the DegP cage structures formed in the presence of chimeric clients. (A) Sections of representative micrographs for the DegP:client complexes and representative 2D class averages. Note that data for the DegP:TrpCage-hTRF1 sample are not shown as this sample was found to consist of nearly all 12mers. A bandpass filter, denoising, and smoothing routines have been applied to better visualize the particles in the micrographs. (B) *Ab-initio* reconstruction maps of the DegP:client complexes identified in (A). The color of a given map matches the DegP:client sample from which it was derived; the 18mer and 24mer maps were both generated from the DegP:His-SUMO-hTRF1 sample. (C) Refinements of the *Ab-initio* maps in (B) with tetrahedral (T), trigonal bipyramidal (D_3), octahedral (O), pentagonal bipyramidal (D_5), and icosahedral (I) symmetry enforced, respectively. Refinements of the *Ab-initio* maps with C_1 symmetry are consistent with those in (B) and (C) and are shown, where relevant, in Figure S6.

(T) symmetry afforded similar maps at 3.5 and 3.1 Å resolution, respectively (Figures 3C, S6A III, S7A). 2D classification of the particle images obtained for the next largest substrate, TrpCage-hTRF1, followed by selection of cage-like 2D classes and *Ab-initio* reconstruction of the selected particles revealed structures similar to those for DegP:hTRF1 (i.e., largely containing 12mer particles, Figure S6B), and thus, the dataset was not subjected to further analysis. For the His-SUMO-hTRF1 dataset, we first performed 2D classification of the particle images (Figures 3A, S5B) followed by subdivision into three populations according to similarity in shape and size (Figure S6C I). *Ab-initio* reconstruction of the subpopulations led to three maps depicting DegP cages: a tetrahedral 12mer (15 nm diameter, ∼22% of the particle selections) analogous to the one derived from the two previous datasets, a trigonal bipyramidal (D_3 symmetry) 18mer (15 and 20 nm along the C_2 and C_3 axes, respectively, ∼12% of particles), and finally, an octahedral (O) 24mer (17 nm diameter, ∼5% of particles, Figures 3B, S6C II). The latter two maps were further refined with either C_1 or higher-order symmetry enforced (D_3 for the 18mer, O for the 24mer), leading to maps with similar features irrespective of the symmetry applied, although, as expected, with increased resolution when higher-order symmetry was enforced (18.1 vs 12.1 Å for the 18mer, 20.1 vs 13.8 Å for the 24mer, Figures 3C, S6C III and IV, S7B). In the presence of IL6-hTRF1, analysis proceeded from 2D classification and selection of classes corresponding to DegP oligomers followed by multiclass *Ab-initio* reconstruction with three classes (Figures 3A, S5C, S6D I and II). Two of the three maps roughly corresponded to 24mers, similar to those found with His-SUMO-hTRF1 (Figure S6D II). The third map was consistent with a novel pentagonal bipyramidal (D_5 symmetry) 30mer cage (24 and 17 nm along the C_2 and C_5 axes, respectively, ∼40% of the selected particles, Figures 3B and S6D II), albeit with poor resolution for one of the constituent trimer panels, pointing to potential structural heterogeneity of this species. This 30mer map was refined with either C_1 or D_5 symmetry leading to maps with 20.5 and 14.1 Å resolution, respectively. Again, these maps depicted similar cages regardless of the symmetry applied (Figures 3C, S6D III and IV, S7C).

For the largest client, MNeon-hTRF1, most of the oligomers within the micrographs were found to be ∼30 nm in diameter (Figures 3A and S5D, white circles). Additionally, we identified less abundant, yet much larger and amorphous DegP assemblies on the order of ∼50−100 nm in size (Figures 3A, S5D, green circles). Selection of the smaller, ∼30 nm particles followed by 2D classification led to class averages with obvious symmetry (Figure S6E I). However, *Ab-initio* reconstruction of the particles from these classes led to a map which, unlike those derived from the other samples, was not of an obviously symmetric DegP oligomer (Figures 3A,B, S5D, S6E I and II). The poor performance of the *Ab-initio* reconstruction in this case could be due to the inability of the algorithm to reconstruct 3D maps of highly symmetric particles,[46] the heterogeneity of the sample, or the somewhat low number of particles in this dataset (note that the assembly of DegP trimers into larger species leads to fewer, higher-order oligomers on the grids). To better define the nature of the particles giving rise to the ∼30 nm map, we performed further refinements with different symmetry groups enforced (Figure S6E III−V). The most realistic result was obtained from a refinement with icosahedral (I) symmetry enforced, which produced a 60mer cage structure (9.7 Å) that was clearly composed of DegP trimer subunits (Figures 3C, S6E IV, S7D). Other symmetry groups (e.g., D_7 symmetry) were ruled out as they failed to produce realistic maps comprised of density consistent with DegP trimers (Figure S6E V). Moreover, 2D projections of the icosahedral symmetry-enforced map closely matched the 2D class averages that were directly calculated from the particle images (Figure S6E VI), providing further confidence in the symmetry of the ∼30 nm species. Finally, we performed a symmetry expansion of the icosahedral map and a local refinement of a single trimeric subunit. This yielded a 5.5 Å map that strongly coincided with the structure of a DegP trimer (Figures S6E VII, and S7D). Taken together, these analyses indicate that in the presence of MNeon-hTRF1, the ∼30 nm oligomers that we observed are most likely a distribution of similarly sized, icosahedral-shaped cage structures that on average contain approximately 60 monomers. Regarding the larger, ∼50−100 nm assemblies identified

https://doi.org/10.1021/jacs.2c11849
J. Am. Chem. Soc. 2023, 145, 13015−13026

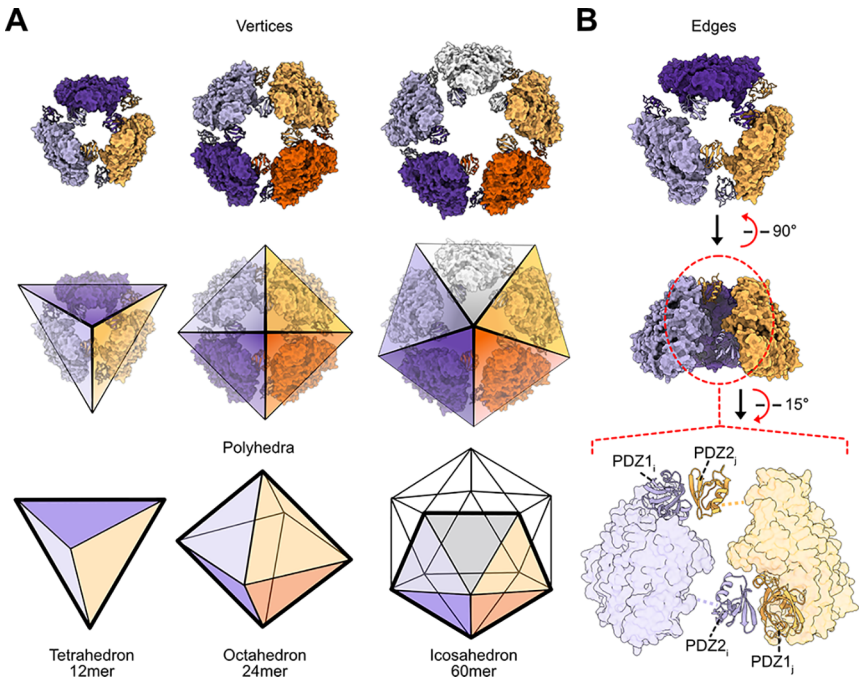

Figure 4. Polyhedral representations of DegP cages. (A, top) DegP cage structures can be approximated as polyhedra by considering the trimer subunits as triangles. Views along the respective 3-, 4-, and 5-fold symmetry axes of the 12mer, 24mer, and 60mer DegP cages from Figure 3C (top and middle; rear subunits are not shown for clarity and representative polyhedral shapes are overlaid in the middle row) highlight that the cage polyhedra (bottom, bold outlines match the edges of the views in the middle row) are assembled via edgewise interactions between trimers. (B) The DegP cage structures are formed by inter-trimer PDZ1^i:PDZ2^j domain interactions. To illustrate, the formation of a single edge connecting light purple and orange trimers in the 12mer (top and middle) occurs through a pair of PDZ1^i:PDZ2^j interactions (bottom).

in the micrographs of this sample (Figures 3A, S5D), we were not able to obtain particle classes with sufficient populations for classification and reconstruction or refinement.

The cryo-EM maps of the 12mer, 18mer, 24mer, 30mer, and 60mer complexes establish that cages are formed through inter-trimer PDZ1^i:PDZ2^j domain interactions, with the protease domain catalytic cores pointing toward the cage interiors (Figures 3C, 4A, S6, and S7), as was found previously in other studies of substrate-engaged DegP assemblies.[18,25,27] In none of the structures were we able to clearly identify DegP's protease domain LA loops (residues 36−81) or the PDZ1-PDZ2 linker sequences (residues 359−374), both of which are known to be highly plastic.[25,47] In addition, there was no obvious density for the N-terminal portions of the chimeric substrates, probably also as a result of their high levels of conformational flexibility and the lower overall resolution of most of the obtained maps in the presence of these clients. An exception was for the 12mer cage structure derived from the DegP:hTRF1 sample, where regions of the bound hTRF1 chains could clearly be identified (see *hTRF1 forms interactions that stabilize the DegP 12mer cage and promote catalysis*).

As illustrated in Figure 4A, each of the DegP structures can be pictured as a polyhedron with triangular faces that correspond to the constituent trimer building blocks. The edges of the polyhedra are formed by inter-trimer PDZ1^i:PDZ2^j domain interactions (Figure 4B top and middle, with edge interactions indicated for the light purple and light orange trimer structures), where the PDZ domain pairings occur at the top and bottom of each edge (Figure 4B bottom showing pairs of ribbon PDZ domains). Different cage sizes, and thus surface curvatures, are created by exploiting these edgewise PDZ domain interactions and the flexible protease-PDZ1 and PDZ1-PDZ2 domain linkers within a protomer that enable an expansion of the gaps in the vertices of the polyhedra (Figure 4A top).

hTRF1 Forms Interactions That Stabilize the DegP 12mer Cage and Promote Catalysis. With the establishment of the general structural features of the DegP cages that are formed using the client proteins discussed above (*Cryo-EM structural studies of DegP cages in the presence of engineered substrates*), we next asked whether specific information could be obtained with reference to DegP:substrate interactions from our cryo-EM data. We focused on the DegP:hTRF1 dataset as it had the most uniform particle distribution and was of the highest overall quality. The trimer map was generated by symmetry expansion of the 12mer map followed by local refinement with a mask over a single trimer, which increased the global resolution from 3.1 to 2.6 Å and enabled building of an atomic model of the trimer structure (Figures 5A, S6A IV, S7A, and S8A). The increase in resolution from the local refinement implies that there is flexibility between different trimer faces. Importantly, at the level of detail afforded by the local refinement, we could clearly identify a number of novel structural interactions between DegP protomers and hTRF1 chains (Figure 5B−D). Well-defined density is observed in the cryo-EM map for the C-terminal halves of the hTRF1 chains (27 residues, Figure 5B; the segments of the hTRF1 chains that could be visualized are shown in pink ribbon, the structure of natively folded hTRF1[32] is shown to the bottom right as a reference with native helices numbered and colored according to the sequence bound to DegP). As mentioned, density was not observed for the N-terminal portions of the hTRF1 chains, presumably due to their flexibility within the cage interiors. The C-terminal halves of hTRF1 clients are arranged in a propeller shape, as shown for the trimer in Figure 5B, where each hTRF1 molecule is bound in a bi-partite manner to the

https://doi.org/10.1021/jacs.2c11849
J. Am. Chem. Soc. 2023, 145, 13015−13026

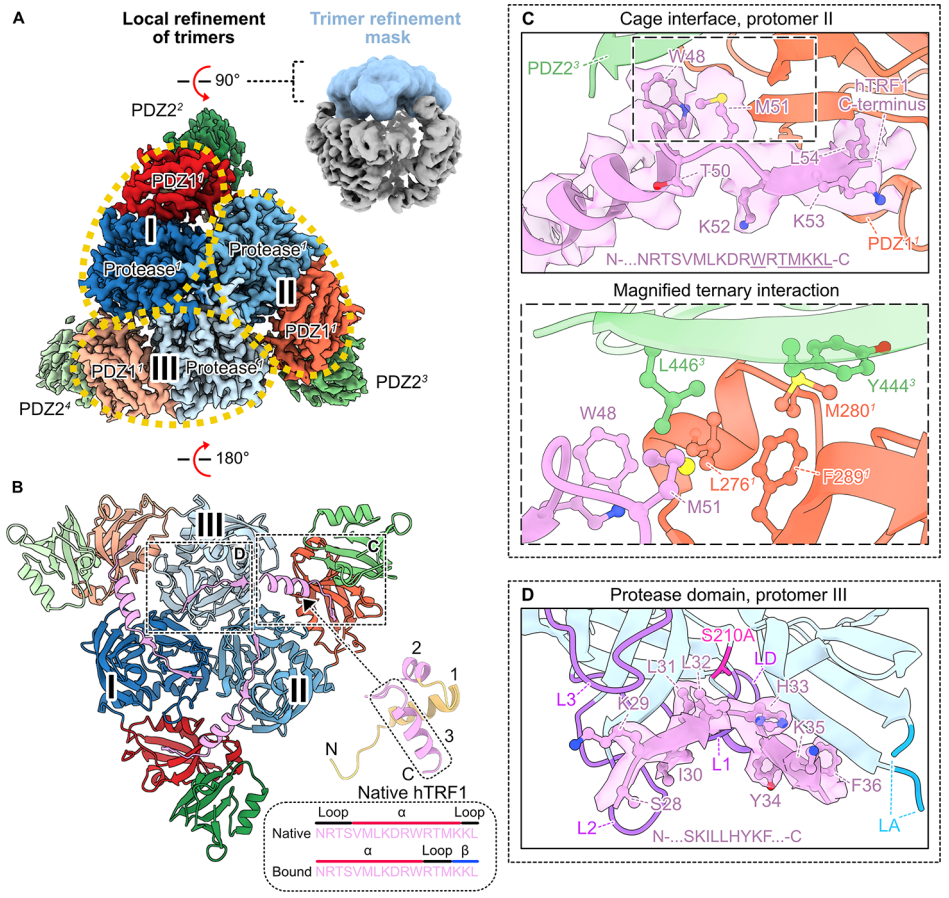

Figure 5. The structure of a 12mer DegP cage reveals interactions between DegP and hTRF1. (A) Cryo-EM density maps for an hTRF1-bound DegP 12mer. Local refinement of a single trimeric face of the 12mer (the refinement mask is indicated in blue in the top right) improved the resolution to 2.6 Å (left). The protease and PDZ1 domains in each of the three protomers (protomers are indicated as I, II, and III) of the displayed trimer (denoted as trimer 1 by the numerical superscript on the domain labels; that is, all 9 domains of the 3 protomers comprising trimer 1 are denoted by 1, those of trimer 2 by 2, and so forth) are outlined with gold ovals and the protomer numbers are indicated in bold. The PDZ2 domains from the protomers within trimer 1 are not visible in this orientation; they form contacts establishing other oligomeric interfaces in the 12mer. PDZ2^{j} domains contributed by trimers 2−4 can be seen along the outside of trimer 1 and are denoted by PDZ2$^{2-4}$ to indicate that they derive from trimers distinct from trimer 1. (B) Structural model of hTRF1 bound to a DegP trimer within the 12mer cage. Counter-clockwise from protomer I, the protease and PDZ1 domains of each protomer in the DegP trimer are shown in dark to light blue (protease domains of successive protomers within the trimer) and red to light orange (successive PDZ1 domains). The PDZ1 domains form PDZ1^{i}:PDZ2^{j} contacts with PDZ2 domains (shown in dark to light green) contributed by protomers from other trimers. The C-terminal portion of hTRF1 that interacts with DegP is shown in pink. For reference, the natively folded hTRF1 structure[32] is shown in the bottom right with the helices numbered and structure colored according to the sequence that we identified as bound to DegP (pink for observed, yellow for not observed). Secondary structure diagrams for residues surrounding and including the third helix in native hTRF1 are indicated at the bottom (enclosed in a smoothed rectangle) to highlight the remodeling of this helix upon binding to DegP. (C, top) Closeup of the cage interface formed by hTRF1 and PDZ1^{1} (protomer II in panel (B)) and PDZ2^{3} domains. The map for the hTRF1 chain at this interface (corresponding to the amino acid sequence indicated at the bottom of the panel) is shown overlaid with the structural model. Residues with well-defined side-chain density have been modeled and are shown as balls and sticks; these are denoted by the underlined portion of the hTRF1 sequence (N-...WRTMKKL-C). Colored balls correspond to side-chain heteroatoms (nitrogen in blue, sulfur in yellow, and oxygen in red). (C, bottom) Expanded region of (C, top) detailing the side chains of hTRF1 and PDZ1^{1} and PDZ2^{3} domains that contribute to the cage interface. (D) Closeup of the interactions between hTRF1 and the protease domain of protomer III from trimer 1 in (B). The hTRF1 sequence for which we observed density is indicated at the bottom of the panel. The catalytic serine is indicated by the red stick (the inactive S210A mutation is employed here). The protease domain L1, L2, L3, and LD loops that have undergone a conformational change upon binding substrate to achieve the catalytically active conformation of DegP are shown in purple. The base of the long LA loop for which we did not observe density is indicated in cyan.

PDZ1 domain of a given protomer and the protease domain of an adjacent protomer (counterclockwise in Figure 5B) within the same trimer. This type of binding mode for DegP clients has previously been proposed based on partial electron density in X-ray studies of peptides engaged to 12mer and 24mer DegP particles.[24,25] Interestingly, we also observed density for the C-terminal half of the hTRF1 chains in the trimer map obtained from the analysis of the ∼30 nm particles in the MNeon-hTRF1 dataset, suggesting that at least for the hTRF1 tag, this binding pose is conserved across dramatically different oligomer sizes (Figure S8B,C).

Interactions between an hTRF1 client molecule and the individual domains of DegP trimers in the context of the 12mer structure are highlighted in Figure 5C,D. The hTRF1 chains are engaged at their C-termini to the peptide-binding clefts of the PDZ1 domains (Figure 5B, with the three PDZ1^{1} domains from trimer 1 shown as red, orange, and light orange ribbon). Docking of each hTRF1 C-terminus (N-...KKL-C,

https://doi.org/10.1021/jacs.2c11849
J. Am. Chem. Soc. 2023, 145, 13015−13026

Figure 5C) is, in part, facilitated by the formation of a non-native β-strand between the C-terminal three residues of hTRF1 and an existing β-strand of the PDZ1 domain whose edge faces the binding groove. These hTRF1 residues that extend the PDZ1 strand comprise the final turn of the client's natively folded 3rd α-helix that is unwrapped upon binding (Figure 5B bottom right, see the secondary structure diagrams for the sequence corresponding to the hTRF1 structure outlined in the dashed box). In addition, the client complex is stabilized through the insertion of hTRF1's terminal Leu side chain and carboxylate group into the peptide-binding pocket. Remarkably, for the segment of the hTRF1 chain that bridges the PDZ1 and protease domain binding sites (i.e., N-...NRTSVMLKDRW...-C), we observed a well-defined helix formed from the majority of the third α-helix in native hTRF1 and several preceding residues from a loop that adopt an additional helix turn when bound to DegP (Figure 5B bottom right, see comparison of native and bound secondary structure diagrams for this segment).

Remodeling of this native hTRF1 helix upon binding to DegP, effectively shifting its register, appears to be important for stabilizing PDZ1^i:PDZ2^j domain interactions between DegP trimers by enabling the formation of a ternary hTRF1:PDZ1^i:PDZ2^j cage interface (Figure 5C). For example, Met51, which in natively folded hTRF1 resides in the final helix (Figure 5B), is restructured so that its side chain contributes to the hydrophobic cage interface formed, as do key residues in the PDZ1^i (Leu276^i, Met280^i, and Phe289^i) and PDZ2^j domains (Tyr444^j and Leu446^j; PDZ2^j domains are shown as dark green, green, and light green ribbon). The side chain of nearby Trp48, which remains in its native helical conformation in the bound form (Figure 5B), also contributes to the packing of this hydrophobic ternary cluster (Figure 5C). Thus, the active restructuring of the client through engagement by DegP directly contributes to the stability of the complex. These ternary hTRF1:PDZ1^i:PDZ2^j interactions also stabilize the packing of PDZ1^i:protease^i domains (Figure 5B), forming a conformation that has been shown to promote the activation of DegP toward bound peptides.[24]

The hTRF1 chain makes a substantial number of additional contacts with the protease domain of a neighboring protomer in the same trimer (Figure 5B,D, protease domains are shown as dark blue, blue, and light blue ribbon). Notably, regions of an hTRF1 chain bound to the protease domain (N-...SKILL-HYKF...-C) form a V-shape through the adoption of two non-native β-strands that extend a pair of β-sheets proximal to the catalytic center of DegP (Figure 5D). This interaction arises through the disruption of native hTRF1's 2nd α-helix (Figure 5B bottom right) and places the hTRF1 chain in a bent conformation with DegP's active site catalytic serine (in this case alanine, red stick in Figure 5D) positioned for efficient proteolysis at the base of the V-shape formed by the hTRF1 peptide backbone. The hTRF1 cleavage products derived from proteolysis by active DegP (Table S2) correlate with the engagement of the hTRF1 chain in this manner. In addition to the well-defined bound-state structure that we identified for the hTRF1 chains, DegP's protease domains were found to be in their catalytically active conformations. This is evidenced by the positions of the L1, L2, L3, and LD loops (Figure 5D purple loops, note that the base of the unobserved LA loop is colored cyan) surrounding the active sites, which permits the alignment of the catalytic centers for client proteolysis.[18]

DISCUSSION

DegP functions as both a protease and a chaperone,[5,10,18,48] playing important housekeeping and virulence-promoting roles in the periplasm of Gram-negative bacterial pathogens. DegP, thus, represents an important antibiotic target,[23] and a recent study has shown that its overactivation by small molecules that mimic the C-terminus of a trimeric OMP client is a viable route for inhibiting bacterial growth.[49] Our structural study of client-engaged DegP oligomers presented here suggests that ternary client:PDZ1^i:PDZ2^j interfaces could be targeted by compounds that augment DegP cage stability to promote enhanced proteolysis, potentially leading to bacterial cell death. Collectively, the many forms of DegP cages that we and others have identified[6,18,25−28] offer a rich structural landscape for potential exploitation in the development of antibacterial therapies.

In this study, we have used a combined DLS/cryo-EM approach to explore the types of cages adopted by DegP in the presence of a series of client proteins with N-terminal domains of increasing hydrodynamic radii. Notably, these techniques have allowed the simultaneous and facile identification of multiple oligomeric species which form in response to the engaged cargo, leading to the identification of a pair of novel structural ensembles. These include pentagonal bipyramidal 30mer and icosahedral 60mer cages, the latter resembling a viral capsid.[50] Particle images were also obtained for DegP assemblies which are on the order of subcellular organelles in diameter (~100 nm), although structures could not be elucidated in this case. Our results establish that DegP can adopt a variety of cage configurations whose sizes depend on the size of the bound substrate and that large biologically relevant substrates can be accommodated. For example, the 60mer and amorphous higher-order DegP assemblies could play roles in the transport of very large cargo within the periplasm, notably virulence factors such as autotransporter proteins whose molecular weights are on the order of 100 kDa.[15,51] Due to their large folded structures, it is thought that autotransporters are kept in a partially unfolded state within the periplasm to facilitate their secretion to the cell exterior.[52,53] The enormous DegP assemblies observed here could serve as protective vesicles that stabilize the denatured state of the autotransporter chain for subsequent secretion.

In a previous study of the structural dynamics of DegP, we showed that an ensemble of complexes was present in solution in the absence of substrate and that this ensemble was likely important to facilitate a timely response to cell stresses that would involve the interaction of the protease-chaperone with a wide range of clients.[28] In the present study, we have highlighted the importance of dynamics in the context of substrate-engaged DegP complexes as well. Notably, an ensemble of different particle types, which can be most simply described in terms of polyhedra, are found for many of the complexes, with the distribution of particle sizes changing in response to the substrate. The oligomeric ensembles identified here may include, in addition to thermodynamically favored completed cages that feature a full complement of 3mers and thus PDZ1^i:PDZ2^j interactions, minor amounts of a number of partly assembled intermediate structures such as bowls[26] or distorted cages composed of sets of 3mers where all possible PDZ1^i:PDZ2^j interactions are not satisfied. Since these would be somewhat similar in size and could in some cases have 2D projections akin to cages, our DLS and cryo-EM analyses

https://doi.org/10.1021/jacs.2c11849
J. Am. Chem. Soc. 2023, 145, 13015−13026

cannot reliably resolve each of these species. Nevertheless, both methodologies pointed to the presence of a variety of particle sizes, and insight into the structures of the dominant oligomer types, in addition to the average and variance of the particle size distribution formed in the presence of a given client, was obtained. We note that while incomplete or strained species that feature a subset of the total number of PDZ1^{i}:PDZ2^{j} interactions can in principle be either smaller or larger than completed DegP cages (e.g., 21mer or 27mer), oligomeric structures which do not contain 3*N* monomers (*N* is the number of 3mers) are not likely to exist in any appreciable amounts due to the high thermal stability of DegP 3mers.[28] In other words, monomers do not readily dissociate from 3mers, biasing against the presence of species such as 22 or 25mers.

The variety of structures that can be achieved with the same trimer building blocks, giving rise to the observed wide variability in particle architectures, derives from the inherent flexibility of the connections between the protease and PDZ domains of a given protomer. Moreover, even in the context of a single oligomer type, for example, the trigonal bipyramidal 30mer or the icosahedral 60mer DegP structures formed with IL6-hTRF1 and MNeon-hTRF1, respectively, there appear to be extensive structural variations, as established by the lower resolution of portions of the *Ab-initio* reconstructed maps for these assemblies in Figure 3B. The lower quality of certain regions of the *Ab-initio* maps probably derives from subunit exchange dynamics (i.e., trimers that interconvert between free and cage-bound conformations giving rise to 27 or 57mers for example), which, in turn, likely stems from the inherent plasticity of the trimer building blocks. This structural variability may be important for reorganization of cage intermediates in the assembly pathway and might also permit the reorientation of bound clients once inside DegP for generating proteolytically competent conformations. It could additionally facilitate client entry and the subsequent egress of cleaved polypeptides. Alternatively, the inherent flexibility of the cages may lead to nuanced structural changes as a function of the number of bound substrates, potentially regulating the function of DegP as either a chaperone or protease.

Compared to the crystallographic studies of DegP assemblies that only observed client density separately in the protease and PDZ1 binding sites,[18,24,25] our structural studies of the 12mer DegP complex in the presence of hTRF1 allowed observation of connectivity both within and between sites on hTRF1 involved in binding, showing that, at least in this case, the bound substrate is not completely unfolded. Indeed, hTRF1's C-terminal half is remodeled to play an active role in stabilizing the structure of the complex through interactions at the PDZ1^{i}:PDZ2^{j} interfaces where the three C-terminal residues of hTRF1 extend an existing PDZ1 β-sheet at the binding site, leading to unwinding of a single turn of a helix in the native hTRF1 structure and subsequent addition of a turn at the opposite helix end. Additionally, catalysis is facilitated through the formation of a V-shaped pose of the hTRF1 chain that is stabilized through the adoption of two non-native hTRF1 β-strands that extend a pair of β-sheets near the catalytic center of DegP. Interestingly, our LC−MS analyses of the hTRF1 cleavage products derived from proteolysis by active DegP (Table S2) indicate that hTRF1 can bind to DegP in more than one register, underscoring a possible functional interplay between bound client dynamics and catalysis. Our activity data in Figure 2E additionally suggest that the structural properties of the N-terminal portions of the chimeric clients influence activity. For example, TrpCage-hTRF1 and IL6-hTRF1 have predominantly α-helical N-terminal "domains" compared to the other chimeras and were less efficiently cleaved by DegP. It may be, therefore, that DegP's proteolytic efficiency is modulated by the folding of the N-terminal regions of the clients, in addition to the structural propensities of their C-terminally bound segments.

This work paints a picture of a highly dynamic DegP—substrate system, with structural flexibility at the level of both receptor and ligand components. DegP assemblies can be thought of as highly dynamic and adaptive cages that are governed by a complex, client-dependent free energy landscape, where cage assemblies redistribute according to the number of bound substrate copies, client sizes, and solution conditions such as temperature. In vivo, DegP cage distributions are most likely constantly in flux within the bacterial periplasm in response to oscillations in misfolded client levels that are the result of a variety of cellular stressors including heat,[5] oxidative,[11] and osmotic shock perturbations.[12] An understanding of the complexities of DegP's free energy landscape is an important first step in the design of molecules to regulate its function and, potentially, to mitigate the virulence of classes of bacterial pathogens.

■ ASSOCIATED CONTENT

Data Availability Statement

All relevant data, outside of structural coordinates, are included in the paper and in the Supporting Information.

Supporting Information

The Supporting Information is available free of charge at https://pubs.acs.org/doi/10.1021/jacs.2c11849.

Protein expression and purification, details of experiments, and data analysis and fitting procedures; representative DLS data, SDS-PAGE analysis of DegP activity, and cryo-EM image processing; and client construct sequences, client cleavage products after exposure to DegP, and details of cryo-EM image processing (PDF)

■ AUTHOR INFORMATION

Corresponding Authors

Robert W. Harkness − *Department of Biochemistry and Department of Molecular Genetics, University of Toronto, Toronto M5S 1A8, Canada; Department of Chemistry, University of Toronto, Toronto M5S 3H6, Canada; Program in Molecular Medicine, The Hospital for Sick Children Research Institute, Toronto M5G 0A4, Canada;* Email: r.harkness@utoronto.ca

Lewis E. Kay − *Department of Biochemistry and Department of Molecular Genetics, University of Toronto, Toronto M5S 1A8, Canada; Department of Chemistry, University of Toronto, Toronto M5S 3H6, Canada; Program in Molecular Medicine, The Hospital for Sick Children Research Institute, Toronto M5G 0A4, Canada;* orcid.org/0000-0002-4054-4083; Email: kay@pound.med.utoronto.ca

Authors

Zev A. Ripstein − *Department of Biochemistry and Department of Molecular Genetics, University of Toronto, Toronto M5S 1A8, Canada; Department of Chemistry, University of Toronto, Toronto M5S 3H6, Canada; Program*

in Molecular Medicine, The Hospital for Sick Children Research Institute, Toronto M5G 0A4, Canada; Present Address: Department of Chemistry, University of Manitoba, Winnipeg R3T 2N2, Canada (Z.A.R.);
orcid.org/0000-0003-3601-0596

Justin M. Di Trani − *Program in Molecular Medicine, The Hospital for Sick Children Research Institute, Toronto M5G 0A4, Canada*

Complete contact information is available at: https://pubs.acs.org/10.1021/jacs.2c11849

Author Contributions

#R.W.H. and Z.A.R. contributed equally to this work.

Funding

This research was funded by a grant from the Canadian Institutes of Health Research, FDN-503573 (L.E.K.).

Notes

The authors declare no competing financial interest.

Electron microscopy maps and atomic models have been deposited to the Electron Microscopy Data Bank and the Protein Data Bank under the accession nos. and PDB ID codes EMD-28781, 8F0U (12mer); EMD-28754, 8F0A (3mer local refinement); EMD-28800, 8F1T (18mer); EMD-28801, 8F1U (24mer); EMD-28806, 8F21 (30mer); EMD-28808, 8F26 (60mer).

■ ACKNOWLEDGMENTS

Dr. John Rubinstein (Hospital for Sick Children, Toronto) is thanked for facilitating the use of a Tecnai F20 microscope and computing resources. R.W.H. and J.M.D.T. are grateful to CIHR and the Hospital for Sick Children Research Institute for post-doctoral fellowships.

■ REFERENCES

(1) Schramm, F. D.; Schroeder, K.; Jonas, K. Protein Aggregation in Bacteria. *FEMS Microbiol. Rev.* **2020**, *44*, 54−72.

(2) Santra, M.; Farrell, D. W.; Dill, K. A. Bacterial Proteostasis Balances Energy and Chaperone Utilization Efficiently. *Proc. Natl. Acad. Sci. U. S. A.* **2017**, *114*, E2654−E2661.

(3) Maisonneuve, E.; Ezraty, B.; Dukan, S. Protein Aggregates: An Aging Factor Involved in Cell Death. *J. Bacteriol.* **2008**, *190*, 6070−6075.

(4) Gottesman, S.; Wickner, S.; Maurizi, M. R. Protein Quality Control: Triage by Chaperones and Proteases. *Genes Dev.* **1997**, *11*, 815−823.

(5) Spiess, C.; Beil, A.; Ehrmann, M. A Temperature-Dependent Switch from Chaperone to Protease in a Widely Conserved Heat Shock Protein. *Cell* **1999**, *97*, 339−347.

(6) Krojer, T.; Ehrmann, M.; Clausen, T.; Garrido-Franco, M.; Huber, R. Crystal Structure of DegP (HtrA) Reveals a New Protease-Chaperone Machine. *Nature* **2002**, *416*, 455−459.

(7) Clausen, T.; Southan, C.; Ehrmann, M. The HtrA Family of Proteases: Implications for Protein Composition and Cell Fate. *Mol. Cell* **2002**, *10*, 443−455.

(8) Toyama, Y.; Harkness, R. W.; Lee, T. Y. T.; Maynes, J. T.; Kay, L. E. Oligomeric Assembly Regulating Mitochondrial HtrA2 Function as Examined by Methyl-TROSY NMR. *Proc. Natl. Acad. Sci. U. S. A.* **2021**, *118*, No. e2025022118.

(9) De Oliveira, D. M. P.; Forde, B. M.; Kidd, T. J.; Harris, P. N. A.; Schembri, M. A.; Beatson, S. A.; Paterson, D. L.; Walker, M. J. Antimicrobial Resistance in ESKAPE Pathogens. *Clin. Microbiol. Rev.* **2020**, *33*, e00181−e00119.

(10) Lipinska, B.; Zylicz, M.; Georgopoulos, C. The HtrA (DegP) Protein, Essential for *Escherichia coli* Survival at High Temperatures, Is an Endopeptidase. *J. Bacteriol.* **1990**, *172*, 1791−1797.

(11) Skórko-Glonek, J.; Zurawa, D.; Kuczwara, E.; Wozniak, M.; Wypych, Z.; Lipinska, B. The *Escherichia coli* Heat Shock Protease HtrA Participates in Defense against Oxidative Stress. *Mol. Gen. Genet.* **1999**, *262*, 342−350.

(12) Leandro, M. R.; Vespoli, L. d. S.; Andrade, L. F.; Soares, F. S.; Boechat, A. L.; Pimentel, V. R.; Moreira, J. R.; Passamani, L. Z.; Silveira, V.; De Souza Filho, G. A. DegP Protease Is Essential for Tolerance to Salt Stress in the Plant Growth-Promoting Bacterium *Gluconacetobacter diazotrophicus* PAL5. *Microbiol. Res.* **2021**, *243*, No. 126654.

(13) Lipinska, B.; Fayet, O.; Baird, L.; Georgopoulos, C. Identification, Characterization, and Mapping of the *Escherichia coli* HtrA Gene, Whose Product Is Essential for Bacterial Growth Only at Elevated Temperatures. *J. Bacteriol.* **1989**, *171*, 1574−1584.

(14) Frees, D.; Brøndsted, L.; Ingmer, H. Bacterial Proteases and Virulence. In *Subcellular Biochemistry*; Dougan, D. A., Ed.; Springer, 2013, *66*, 161−192.

(15) Ruiz-Perez, F.; Henderson, I. R.; Leyton, D. L.; Rossiter, A. E.; Zhang, Y.; Nataro, J. P. Roles of Periplasmic Chaperone Proteins in the Biogenesis of Serine Protease Autotransporters of *Enterobacteriaceae*. *J. Bacteriol.* **2009**, *191*, 6571−6583.

(16) Purdy, G. E.; Hong, M.; Payne, S. M. *Shigella flexneri* DegP Facilitates IcsA Surface Expression and Is Required for Efficient Intercellular Spread. *Infect. Immun.* **2002**, *70*, 6355−6364.

(17) Purdy, G. E.; Fisher, C. R.; Payne, S. M. IcsA Surface Presentation in *Shigella flexneri* Requires the Periplasmic Chaperones DegP, Skp, and SurA. *J. Bacteriol.* **2007**, *189*, 5566−5573.

(18) Krojer, T.; Sawa, J.; Schäfer, E.; Saibil, H. R.; Ehrmann, M.; Clausen, T. Structural Basis for the Regulated Protease and Chaperone Function of DegP. *Nature* **2008**, *453*, 885−890.

(19) Braselmann, E.; Chaney, J. L.; Champion, M. M.; Clark, P. L. DegP Chaperone Suppresses Toxic Inner Membrane Translocation Intermediates. *PLoS One* **2016**, *11*, No. e0162922.

(20) Sklar, J. G.; Wu, T.; Kahne, D.; Silhavy, T. J. Defining the Roles of the Periplasmic Chaperones SurA, Skp, and DegP in *Escherichia coli*. *Genes Dev.* **2007**, *21*, 2473−2484.

(21) Confer, A. W.; Ayalew, S. The OmpA Family of Proteins: Roles in Bacterial Pathogenesis and Immunity. *Vet. Microbiol.* **2013**, *163*, 207−222.

(22) Baud, C.; Hodak, H.; Willery, E.; Drobecq, H.; Locht, C.; Jamin, M.; Jacob-Dubuisson, F. Role of DegP for Two-Partner Secretion in *Bordetella*. *Mol. Microbiol.* **2009**, *74*, 315−329.

(23) Kim, S.; Sauer, R. T. Distinct Regulatory Mechanisms Balance DegP Proteolysis to Maintain Cellular Fitness during Heat Stress. *Genes Dev.* **2014**, *28*, 902−911.

(24) Krojer, T.; Sawa, J.; Huber, R.; Clausen, T. HtrA Proteases Have a Conserved Activation Mechanism That Can Be Triggered by Distinct Molecular Cues. *Nat. Struct. Mol. Biol.* **2010**, *17*, 844−852.

(25) Kim, S.; Grant, R. A.; Sauer, R. T. Covalent Linkage of Distinct Substrate Degrons Controls Assembly and Disassembly of DegP Proteolytic Cages. *Cell* **2011**, *145*, 67−78.

(26) Shen, Q.-T.; Bai, X.-C.; Chang, L.-F.; Wu, Y.; Wang, H.-W.; Sui, S.-F. Bowl-Shaped Oligomeric Structures on Membranes as DegP's New Functional Forms in Protein Quality Control. *Proc. Natl. Acad. Sci. U. S. A.* **2009**, *106*, 4858−4863.

(27) Sui, S.-F.; Zhang, X.; Jiang, J.; Chang, Z.; Wu, Y.; Zhou, Z. H.; Chen, Y. Activation of DegP Chaperone-Protease via Formation of Large Cage-like Oligomers upon Binding to Substrate Proteins. *Proc. Natl. Acad. Sci. U. S. A.* **2008**, *105*, 11939−11944.

(28) Harkness, R. W.; Toyama, Y.; Ripstein, Z. A.; Zhao, H.; Sever, A. I. M.; Luan, Q.; Brady, J. P.; Clark, P. L.; Schuck, P.; Kay, L. E. Competing Stress-Dependent Oligomerization Pathways Regulate Self-Assembly of the Periplasmic Protease-Chaperone DegP. *Proc. Natl. Acad. Sci. U. S. A.* **2021**, *118*, No. e2109732118.

(29) Dautin, N. Serine Protease Autotransporters of *Enterobacteriaceae* (SPATEs): Biogenesis and Function. *Toxins* **2010**, *2*, 1179−1206.

(30) Junker, M.; Besingi, R. N.; Clark, P. L. Vectorial Transport and Folding of an Autotransporter Virulence Protein during Outer Membrane Secretion. *Mol. Microbiol.* **2009**, *71*, 1323−1332.
(31) Iwanczyk, J.; Damjanovic, D.; Kooistra, J.; Leong, V.; Jomaa, A.; Ghirlando, R.; Ortega, J. Role of the PDZ Domains in *Escherichia coli* DegP Protein. *J. Bacteriol.* **2007**, *189*, 3176−3186.
(32) Nishikawa, T.; Nagadoi, A.; Yoshimura, S.; Aimoto, S.; Nishimura, Y. Solution Structure of the DNA-Binding Domain of Human Telomeric Protein, HTRF1. *Structure* **1998**, *6*, 1057−1065.
(33) Merdanovic, M.; Burston, S. G.; Schmitz, A. L.; Köcher, S.; Knapp, S.; Clausen, T.; Kaiser, M.; Huber, R.; Ehrmann, M. Activation by Substoichiometric Inhibition. *Proc. Natl. Acad. Sci. U. S. A.* **2020**, *117*, 1414−1418.
(34) Nishikawa, T.; Okamura, H.; Nagadoi, A.; König, P.; Rhodes, D.; Nishimura, Y. Solution Structure of a Telomeric DNA Complex of Human TRF1. *Structure* **2001**, *9*, 1237−1251.
(35) Neidigh, J. W.; Fesinmeyer, R. M.; Andersen, N. H. Designing a 20-Residue Protein. *Nat. Struct. Biol.* **2002**, *9*, 425−430.
(36) Mossessova, E.; Lima, C. D. Ulp1-SUMO Crystal Structure and Genetic Analysis Reveal Conserved Interactions and a Regulatory Element Essential for Cell Growth in Yeast. *Mol. Cell* **2000**, *5*, 865−876.
(37) Xu, G. Y.; Yu, H. A.; Hong, J.; Stahl, M.; McDonagh, T.; Kay, L. E.; Cumming, D. A. Solution Structure of Recombinant Human Interleukin-6. *J. Mol. Biol.* **1997**, *268*, 468−481.
(38) Clavel, D.; Gotthard, G.; Von Stetten, D.; De Sanctis, D.; Pasquier, H.; Lambert, G. G.; Shaner, N. C.; Royant, A. Structural Analysis of the Bright Monomeric Yellow-Green Fluorescent Protein MNeonGreen Obtained by Directed Evolution. *Acta Crystallogr. Sect. D: Struct. Biol.* **2016**, *72*, 1298−1307.
(39) Attri, A. K.; Fernández, C.; Minton, A. P. Self-Association of Zn-Insulin at Neutral PH: Investigation by Concentration Gradient-Static and Dynamic Light Scattering. *Biophys. Chem.* **2010**, *148*, 23−27.
(40) Mailer, A. G.; Clegg, P. S.; Pusey, P. N. Particle Sizing by Dynamic Light Scattering: Non-Linear Cumulant Analysis. *J. Phys. Condens. Matter* **2015**, *27*, No. 145102.
(41) Hanlon, A. D.; Larkin, M. I.; Reddick, R. M. Free-Solution, Label-Free Protein-Protein Interactions Characterized by Dynamic Light Scattering. *Biophys. J.* **2010**, *98*, 297−304.
(42) Frisken, B. J. Revisiting the Method of Cumulants for the Analysis of Dynamic Light-Scattering Data. *Appl. Opt.* **2001**, *40*, 4087−4091.
(43) Koppel, D. E. Analysis of Macromolecular Polydispersity in Intensity Correlation Spectroscopy: The Method of Cumulants. *J. Chem. Phys.* **1972**, *57*, 4814−4820.
(44) Strauch, K. L.; Beckwith, J. An *Escherichia coli* Mutation Preventing Degradation of Abnormal Periplasmic Proteins. *Proc. Natl. Acad. Sci. U. S. A.* **1988**, *85*, 1576−1580.
(45) Lorber, B.; Fischer, F.; Bailly, M.; Roy, H.; Kern, D. Protein Analysis by Dynamic Light Scattering: Methods and Techniques for Students. *Biochem. Mol. Biol. Educ.* **2012**, *40*, 372−382.
(46) Punjani, A.; Rubinstein, J. L.; Fleet, D. J.; Brubaker, M. A. CryoSPARC: Algorithms for Rapid Unsupervised Cryo-EM Structure Determination. *Nat. Methods* **2017**, *14*, 290−296.
(47) Sobiecka-Szkatula, A.; Polit, A.; Scire, A.; Gieldon, A.; Tanfani, F.; Szkarlat, Z.; Ciarkowski, J.; Zurawa-Janicka, D.; Skorko-Glonek, J.; Lipinska, B. Temperature-Induced Conformational Changes within the Regulatory Loops L1-L2-LA of the HtrA Heat-Shock Protease from *Escherichia coli*. *Biochim. Biophys. Acta* **2009**, *1794*, 1573−1582.
(48) Swamy, K. H. S.; Chung, C. H.; Goldberg, A. L. Isolation and Characterization of Protease Do from *Escherichia coli*, a Large Serine Protease Containing Multiple Subunits. *Arch. Biochem. Biophys.* **1983**, *224*, 543−554.
(49) Cho, H.; Choi, Y.; Min, K.; Son, J. B.; Park, H.; Lee, H. H.; Kim, S. Over-Activation of a Nonessential Bacterial Protease DegP as an Antibiotic Strategy. *Commun. Biol.* **2020**, *3*, 547.
(50) Kaufmann, B.; Simpson, A. A.; Rossmann, M. G. The Structure of Human Parvovirus B19. *Proc. Natl. Acad. Sci. U. S. A.* **2004**, *101*, 11628−11633.
(51) Khan, S.; Mian, H. S.; Sandercock, L. E.; Chirgadze, N. Y.; Pai, E. F. Crystal Structure of the Passenger Domain of the *Escherichia coli* Autotransporter EspP. *J. Mol. Biol.* **2011**, *413*, 985−1000.
(52) Junker, M.; Schuster, C. C.; McDonnell, A. V.; Sorg, K. A.; Finn, M. C.; Berger, B.; Clark, P. L. Pertactin Beta-Helix Folding Mechanism Suggests Common Themes for the Secretion and Folding of Autotransporter Proteins. *Proc. Natl. Acad. Sci. U. S. A.* **2006**, *103*, 4918−4923.
(53) Oliver, D. C.; Huang, G.; Nodel, E.; Pleasance, S.; Fernandez, R. C. A Conserved Region within the *Bordetella pertussis* Autotransporter BrkA Is Necessary for Folding of Its Passenger Domain. *Mol. Microbiol.* **2003**, *47*, 1367−1383.

Recommended by ACS

Converting a Natural-Light-Driven Outward Proton Pump Rhodopsin into an Artificial Inward Proton Pump
María del Carmen Marín, Keiichi Inoue, *et al.*
APRIL 21, 2023
JOURNAL OF THE AMERICAN CHEMICAL SOCIETY
READ

Sequential Unfolding Mechanisms of Monomeric Caspases
Isha Joglekar and A. Clay Clark
MAY 31, 2023
BIOCHEMISTRY
READ

Rational Construction of Protein-Mimetic Nano-Switch Systems Based on Secondary Structure Transitions of Synthetic Polypeptides
Chenglong Ge, Lichen Yin, *et al.*
MAY 11, 2023
JOURNAL OF THE AMERICAN CHEMICAL SOCIETY
READ

Conformational Flexibility Is a Key Determinant for the Lytic Activity of the Pore-Forming Protein, Cytolysin A
Avijeet Kulshrestha, K. Ganapathy Ayappa, *et al.*
DECEMBER 21, 2022
THE JOURNAL OF PHYSICAL CHEMISTRY B
READ

Get More Suggestions >

https://doi.org/10.1021/jacs.2c11849
J. Am. Chem. Soc. 2023, 145, 13015−13026